GSA Data Repository 2019220

Schachtman, N.S., et al., 2019, The interplay between physical and chemical erosion over glacial-interglacial cycles: Geology, https://doi.org/10.1130/G45940.1

Materials and Methods

Site selection and sampling

Using LiDAR imagery, we identified representative ridgetops in the ~6 km^2 Little Lake catchment from which to sample the modern soil column. By targeting the ridgetops, we sampled material weathered in place (Riebe et al., 2004; Green et al., 2006). At each soil pit, we measured the depth to saprolite, described horizon development and collected samples for bulk density measurements. We sampled weakly developed inceptisols, characterized by a 0-2 cm thick organic rich O-horizon, transitioning into a 0.3 to 0.7 m thick B_w Horizon (layer of mobile regolith), and finally a weathered, oxidized saprolitic sandstone layer, which extended well below the surface. The interface between the soil and saprolite was defined by the transition from mobile regolith to regolith weathered in place that still maintained some bedrock structure. At each pit, we sampled equal volumes of bulk soil every 10 cm along a vertical profile (discarding material from the O horizon), combining the samples for an average geochemical characterization at each locale (Larsen et al., 2014). We also sampled saprolite material underlying each soil pit. We took additional samples of saprolite material from road cuts in the area and confirmed that they were geochemically similar to our saprolite samples from the soil pits.

To obtain fresh bedrock samples that we believe reflect the parent material, we sampled the bedrock channel thalweg found just downstream of the lake (Rempe and Dietrich, 2014), at a location below the level of late summer base flow. After an extensive search, this was the only location where we could confidently characterize and sample largely unaltered Eocene age Tyee sandstone, a sequence of deltaic and turbidite sands (Ryu, 2003). Additionally, samples from this location were the only bedrock samples not extensively more weathered than our LG sediment samples. Thus, these samples are likely an accurate representation of the LG parent material, compared to the weathered bedrock that currently underlies the modern soil profile. These bedrock samples were collected in several dispersed locations, chiefly roadcuts and soil pits,

throughout the catchment (Fig 1). Our trace and major element concentrations of these bedrock samples show similarity to fresh Tyee sandstone samples from Coos Bay, which is > 150 km from our study area (Anderson et al., 2002), and point counts of thin sections from across a large area show similar compositions of quartz, feldspar, and lithic fragments. Combined with the characteristic topography and landforms across western Oregon and Cascadia, this argues for the regional significance of our findings. Also, because of these common properties, we analyze trace element concentrations in the sediment core to show systematic variations over the 50-kyr record.

We sampled lake sediment from two previously dated and characterized cores extracted from the Little Lake catchment in 2010 (Marshall et al., 2015, Marshall et al., 2017). Smear slide analysis on sediment from a variety of different intervals revealed that sediment is primarily of detrital origin, with some mixed organics and macrofossils. For geochemical analysis, we sampled ~2-4 cm intervals of lake sediment throughout the ~70 m of total core, focusing our sampling on representative sediment from the Late Holocene (LH; < 2.5 ka) and LG intervals. In preparation for grain size analysis, we sampled approximately 0.5 cm^3 of material from these same intervals. Particle sizes were analyzed using a Malvern laser diffraction grain size analyzer and grain size separations of soil and lake sediment were completed using an automated sieve shaker. Generally, sediment from the LG interval is poorly sorted and consists of fine to medium sand, with 1%-5% organic matter. the core samples we analyzed in this study reveal minimal evidence of sediment sorting, reworking, or sedimentary structures and typically exhibit an unsorted character reflective of rapid delivery. Sediment from the LH is primarily silt and fine sand, with 5%-12% organic matter.

Analytical procedures

We dried soil, sediment and bedrock samples overnight at 60 °C to remove water and combusted them at 550 °C for 10-12 hours (depending on sample size) to eliminate organic material before geochemical analysis (Heiri et al., 2001). Major element concentrations in sample were measured by X-ray fluorescence (XRF) following a lithium borate fusion, while trace element concentrations were measured by pressed pellet XRF method at ALS Minerals, Reno, NV. Particle sizes were analyzed at California State University-Fullerton using a Malvern

laser diffraction grain size analyzer, following removal of organic material by H_2O_2. Grain size separations of soil and lake sediment were completed using an automated sieve shaker.

Modern and past dust deposition

Observed and modeled rates of dust deposition during the last glacial and modern are estimated at 2 to 4 and 0.5 to 1.0 gm m^{-2} yr^{-1}, respectively (Maher et al., 2010). After converting observed soil production and erosion rates (Heimsath et al., 2001) assuming a conservative bulk density of 2.0 gm cm^{-3}, we obtain rates of ~200 gm m^{-2} yr^{-1}. Although very high (>200 gm m^{-2} yr^{-1}) dust deposition rates are recovered in LG sediments in the midwestern US and downstream of glaciers, these high rates reflect proximal sources that are not relevant to our study area.

Chemical weathering Intensity and chemical weathering fluxes

To assess the intensity of weathering at our site, we utilize the chemical depletion fraction (CDF; Riebe et al., 2001) to determine the relative contribution of chemical denudation (W) to total denudation (D). This calculation relies on the assumption that trace elements (in this case, Zr) are chemically inert during the weathering process such that

$$\mathrm{CDF} = 1 - \left(\frac{[\mathrm{Zr}]_{\mathrm{rock}}}{[\mathrm{Zr}]_{\mathrm{soil}}}\right). \quad \text{(S1)}$$

We combine previously measured cosmogenic ^{10}Be denudation rates (Marshall et al., 2017; D, units L T^{-1}) with estimated CDF values to derive a chemical weathering rate (W, units L T^{-1}),

$$W = D\,(\mathrm{CDF}). \quad \text{(S2)}$$

Major element concentrations were used to calculate the Chemical Index of Alteration (CIA; Nesbitt and Young, 1982),

$$CIA = \left[\frac{\mathrm{Al_2O_3}}{\mathrm{Al_2O_3 + CaO + K_2O + Na_2O}}\right] \mathrm{x100}. \quad \text{(S3)}$$

References

Anderson, S.P., Dietrich, W.E., and Brimhall, G.H., 2002, Weathering profiles, mass-balance analysis, and rates of solute loss: Linkages between weathering and erosion in a small, steep catchment: Bulletin of the Geological Society of America, v. 114, no. 9, p. 1143–1158, doi: 10.1130/0016-7606(2002)114<1143:WPMBAA>2.0.CO.

Green, E.G., Dietrich, W.E., and Banfield, J.F., 2006, Quantification of chemical weathering rates across an actively eroding hillslope: Earth and Planetary Science Letters, v. 242, no. 1, p. 155–169, doi: 10.1016/j.epsl.2005.11.039.

Heiri, O., Lotter, A.F., and Lemcke, G., 2001, Loss on ignition as a method for estimating organic and carbonate content in sediments: reproducibility and comparability of results: Journal of Paleolimnology, v. 25, no. 1, p. 101–110, doi: 10.1023/A:1008119611481.

Larsen, I.J., Almond, P.C., Eger, A., Stone, J.O., Montgomery, D.R., and Malcolm, B., 2014, Rapid soil production and weathering in the Southern Alps, New Zealand.: Science, v. 343, no. 6171, p. 637–640, doi: 10.1126/science.124490.

Maher, B.A., Prospero, J.M., Mackie, D., Gaiero, D., Hesse, P.P. and Balkanski, Y., 2010. Global connections between aeolian dust, climate and ocean biogeochemistry at the present day and at the last glacial maximum. Earth-Science Reviews, v. 99, no. 1-2, pp.61-97, doi: 10.1016/j.earscirev.2009.12.001.

Marshall, J.A., Roering, J.J., Bartlein, P.J., Gavin, D.G., Granger, D.E., Rempel, A.W.,Praskievicz, S.J., and Hales, T.C., 2015, Frost for the trees: Did climate increase erosion in unglaciated landscapes during the late Pleistocene? Science Advances, v. 1, no. 10, p.e1500715–e1500715, doi: 10.1126/sciadv.1500715.

Marshall, J.A., Roering, J.J., Gavin, D.G., and Granger, D.E., 2017, Late Quaternary climatic controls on erosion rates and geomorphic processes in western Oregon, USA: Geological Society of America Bulletin, v. 129, no. 5–6, p. 715–731, doi: 10.1130/B31509.1.

Nesbitt, H.W., and Young, G.M., 1982, Early Proterozoic climates and plate motions inferred from major element chemistry of lutites: Nature, v. 299, no. 5885, p. 715–717, doi: 10.1038/299715a0.

Rempe, D.M., and Dietrich, W.E., 2014, A bottom-up control on fresh-bedrock topography under landscapes.: Proceedings of the National Academy of Sciences of the United States of America, v. 111, no. 18, p. 6576–81, doi: 10.1073/pnas.1404763111.

Riebe, C.S., Kirchner, J.W., Granger, D.E., and Finkel, R.C., 2001, Strong tectonic and weak climatic control of long term chemical weathering rates: Geology, no. 29, p. 511–514, doi: 10.1130/0091-7613(2001)029<0511:STAWCC>2.0.CO;2.

Riebe, C.S., Kirchner, J.W., and Finkel, R.C., 2004, Sharp decrease in long-term chemical weathering rates along an altitudinal transect: Earth and Planetary Science Letters, v. 218, no. 3–4, p. 421–434, doi: 10.1016/S0012-821X(03)00673-3.

Ryu, I.C., 2003, Petrography, diagenesis and provenance of Eocene Tyee Basin sandstones, southern Oregon Coast range: New view from sequence stratigraphy: Island Arc, v. 12, no. 4, p. 398–410, doi: 10.1046/j.1440-1738.2003.00409.x.

Supplemental Figures

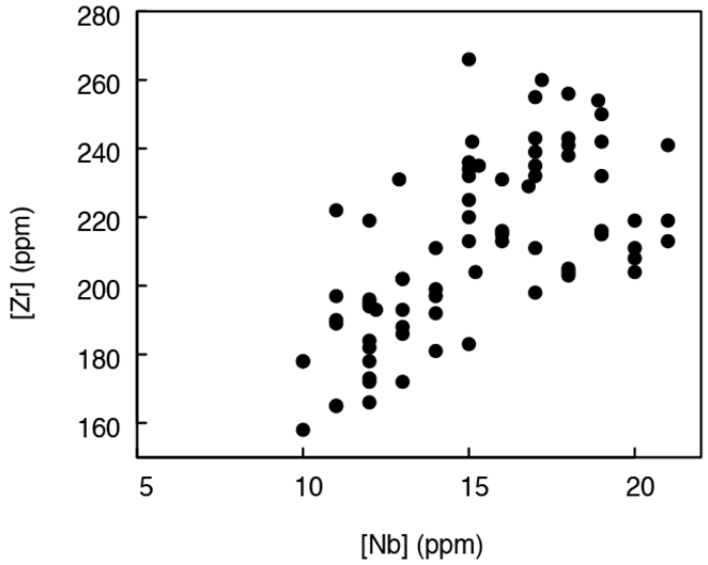

Figure DR1. Zr versus Nb for soil, sediment and parent material samples. The positive correlation between Zr and Nb indicates that these trace elements covary and thus reflect similar weathering behavior.

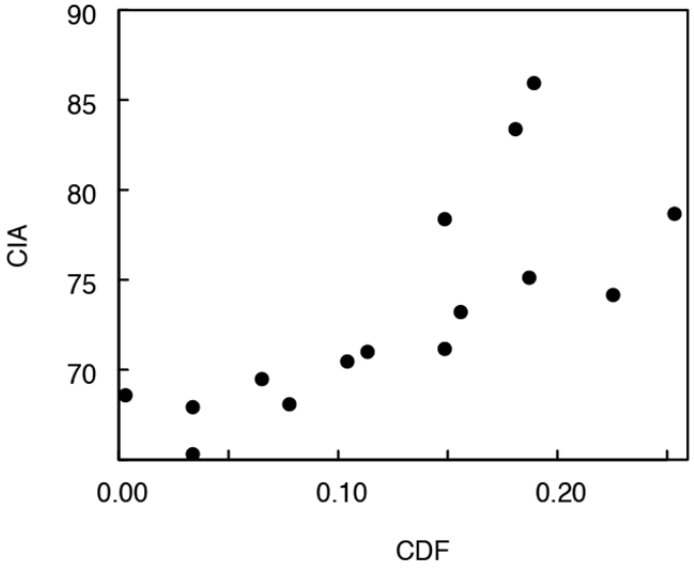

Figure DR2. Chemical Index of Alteration (CIA; eq. S3) versus Chemical Depletion Fraction (CDF; eq. S1) values for soil and lake sediment samples. The two independent weathering indices show a strong positive correlation, suggesting that calculated CIA values from bedrock, soil, and sediment, Zr provide a first order estimation of chemical weathering intensity at our study site.

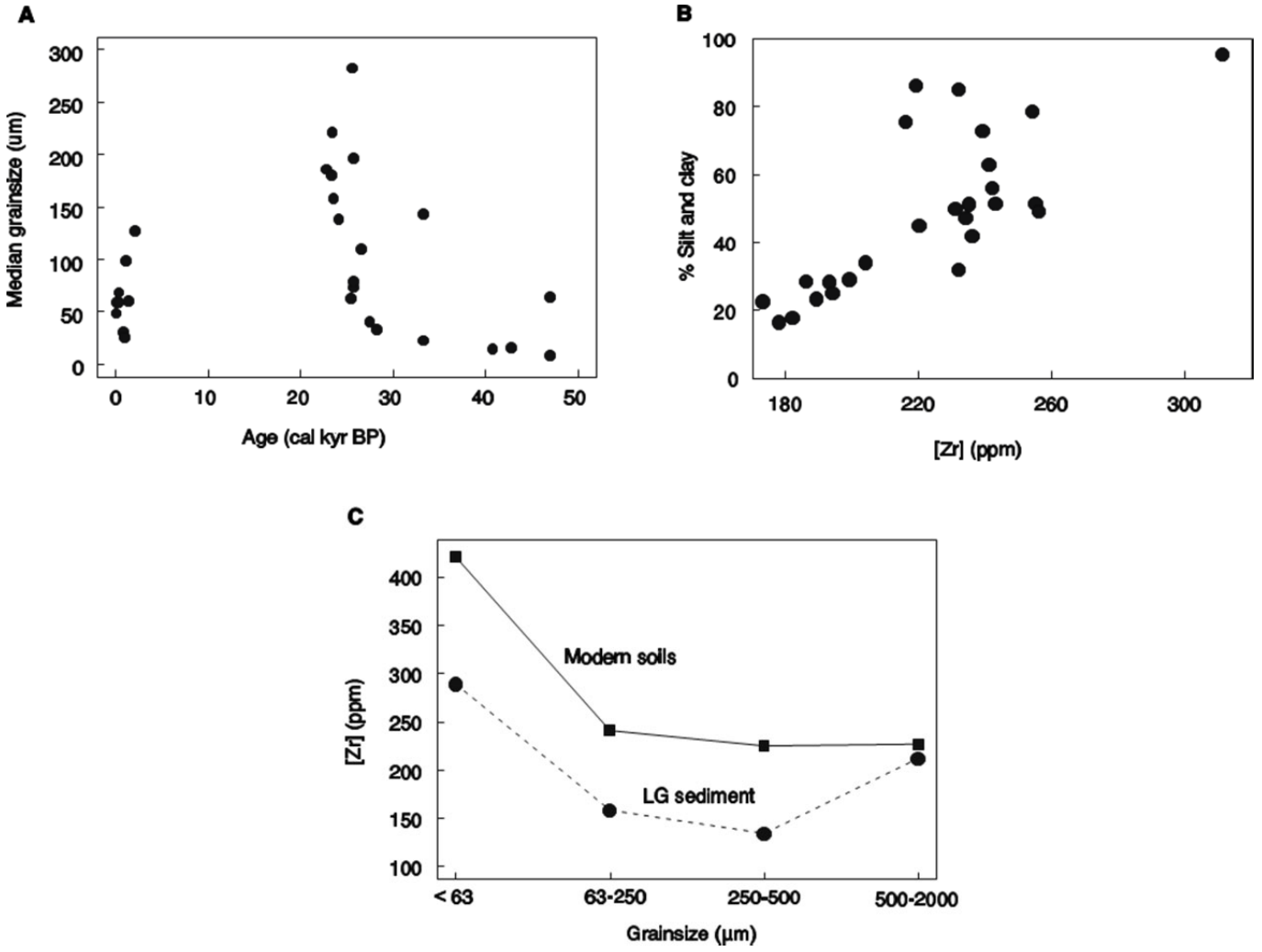

Figure DR3. (**A**) Median grain size versus age (kyr cal BP). Note a large excursion in median grain size during the LG interval, attributed to a shift in geomorphic process and/or transport regime and a low chemical weathering intensity in the soils**.** (**B**) % clay and silt versus Zr. (**C**) Zr for a range of grain sizes in a modern soil (squares, black line) and an LG sediment sample (circles, dashed line). Note that Zr is depleted relative to modern soil for all grain sizes below 500 µm. Grain size class names: silt-clay (<63 µm), fine sand (63-250 µm), medium sand (250-500 µm), and coarse to very coarse sand (500-2000 µm).

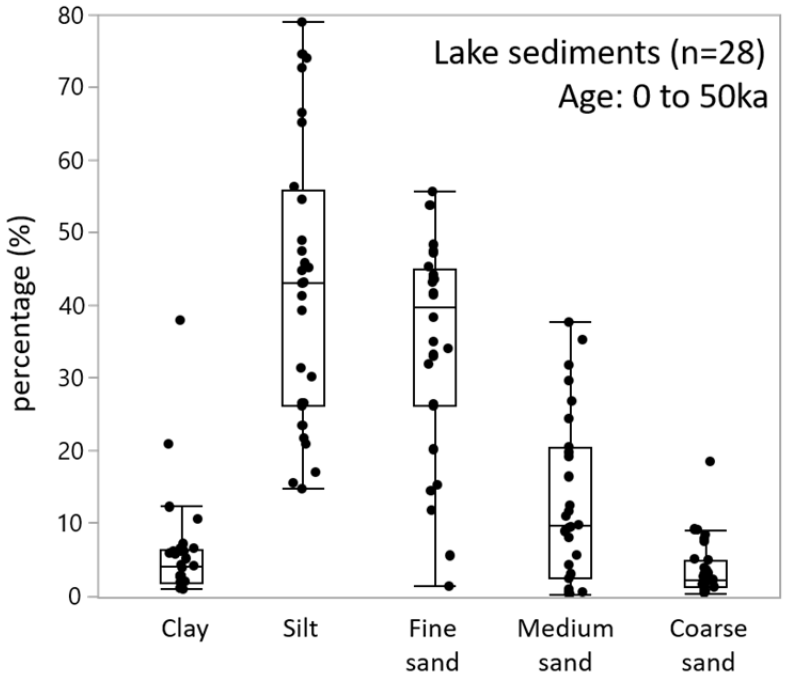

Figure DR4. Proportion of grain size classes (by mass fraction) for 28 lake sediment samples used in this analysis. Note that silt to medium sand grain size classes constitute the vast majority of sediment samples. Importantly, the signature of chemical depletion (as quantified by CDF) in these size classes is consistent (Fig. DR3).

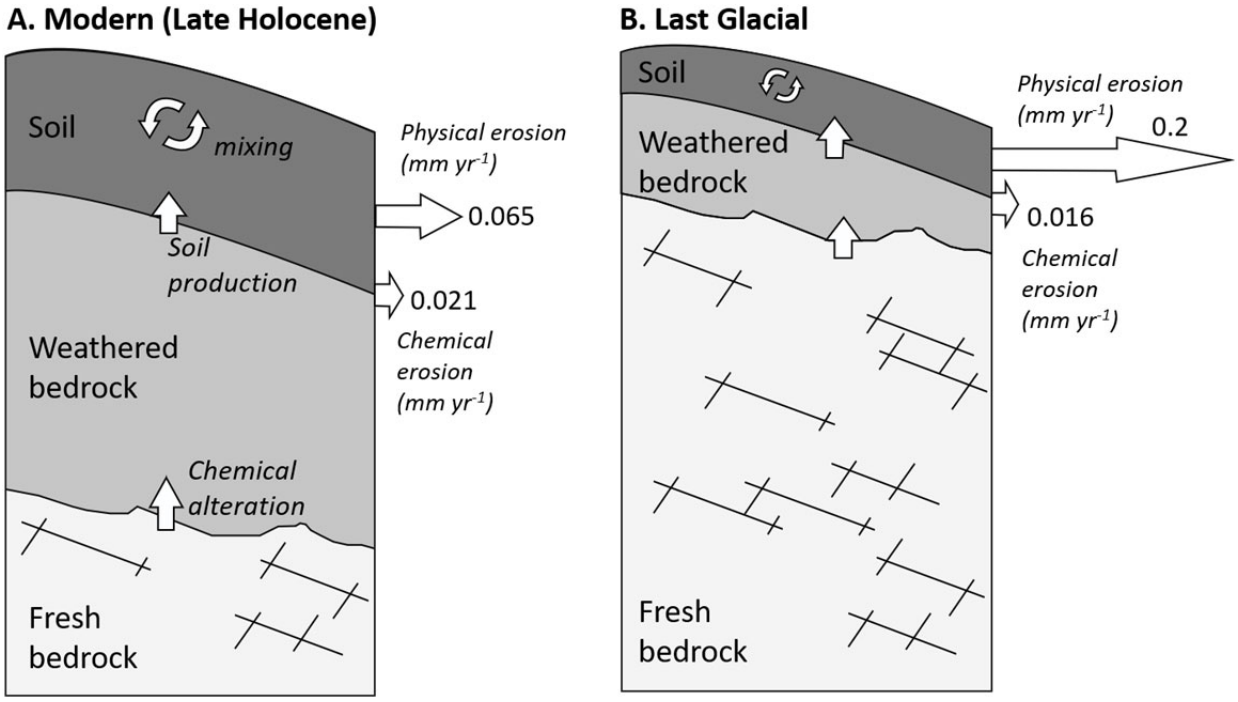

Figure DR5. Schematic depiction of potential critical zone architecture characteristic of the Last Glacial and today, which is roughly equivalent to the Late Holocene given the millenia-scale integration time of soil properties and erosion rate estimates. The arrows are scaled to represent physical and chemical erosion fluxes and when added together these equal the denudation (or total erosion) rate generated by in-situ ^{10}Be analysis. Note that chemical weathering takes place in both weathered bedrock and soil in both cases.

Table DR1. Soil pit and bedrock sample locations.

Sample site ID	Lat.	Lon.	Depth to bedrock (cm)
Soil			
LLS1	44.17252	-123.60545	40
LLS2	44.16725	-123.60925	45
LLS3	44.1666	-123.6094	38
LLS4	44.17632	-123.60547	55
LLS6	44.16625	-123.60437	40
LLS7	44.1608	-123.60332	60
LLS8	44.1608	-123.60332	34
Bedrock			
LLB1 (weathered)	44.172277	-123.60449	
LLB2 (weathered)	44.172277	-123.60449	
LLB3 (weathered)	44.16494	-123.61264	
LLB4 (weathered)	44.16494	-123.61264	
LLB5 (weathered)	44.16777	-123.61266	
LLB6 (weathered)	44.16777	-123.61266	
LLB7 (weathered)	44.158824	-123.572814	
LLB8 (weathered)	44.158824	-123.572814	
LLB7b (weathered)	44.158824	-123.572814	
LLB9 (weathered)	44.15974	-123.60165	
LLB10 (weathered)	44.15974	-123.60165	
LLB11 (weathered)	44.15722	-123.59616	
LLB12 (weathered)	44.15722	-123.59616	
LLB13 (fresh)	44.15773	-123.57455	
LLB14 (fresh)	44.15773	-123.57455	
LLB15a (fresh)	44.15773	-123.57455	
LLB15b (fresh)	44.15773	-123.57455	

Table DR2. Major and trace element X-ray fluorescence data for weathered and fresh bedrock samples.

Sample ID	Al_2O_3 (%)	BaO (%)	CaO (%)	Cr_2O_3 (%)	Fe_2O_3 (%)	K_2O (%)	MgO (%)	MnO (%)	Na_2O (%)	P_2O_5 (%)	SO_3 (%)	SiO_2 (%)	SrO (%)	TiO_2 (%)	LOI (%)	Nb (ppm)	Zr (ppm)	Be (ppm)
LLB1	14.76	0.08	3.12	0.01	4.53	2.17	2.15	0.05	2.9	0.15	0.02	67.16	0.05	0.54	1.59	11	190	1.57
LLB2	17.08	0.07	1.81	0.01	7.44	2.63	3.8	0.03	1.72	0.13	0.84	61.21	0.03	0.78	2.85	14	181	2.58
LLB3	15.5	0.09	2.7	0.01	4.11	2.69	1.98	0.04	2.79	0.16	0.28	67.66	0.05	0.59	1.37	12	196	1.86
LLB4	16.78	0.08	2.78	0.01	7.3	2.84	3.65	0.06	2.05	0.14	1.12	60.15	0.04	0.77	2.78	15	183	2.5
LLB5	14.98	0.1	3.6	0.01	4	2.22	1.55	0.09	3.09	0.16	0.02	67.36	0.06	0.57	1.51	11	197	1.58
LLB6	14.29	0.09	4.43	0.01	5.12	2.11	2.09	0.17	2.87	0.16	0.02	65.41	0.05	0.61	2.33	11	222	1.52
LLB7	14.88	0.1	2.66	0.01	3.31	2.82	1.07	0.08	3.33	0.15	0.03	70.03	0.05	0.55	0.49	13	202	1.69
LLB7b	17.13	0.09	1.9	0.01	6.38	3.28	2.27	0.07	2.44	0.13	0.03	63.4	0.05	0.64	1.73	17	198	2.75
LLB8	17.02	0.1	2.13	0.01	5.8	3.3	2.31	0.07	2.59	0.14	0.05	64.14	0.05	0.64	1.44	18	203	2.65
LLB11																13	193	
LLB12																14	192	
LLB13																12	178	
LLB14																13	172	
LLB15a																12	172	
LLB15b																12	166	

Table DR3. Major and trace element X-ray fluorescence data for soil samples.

Pit ID	Al_2O_3 (%)	BaO (%)	CaO (%)	Cr_2O_3 (%)	Fe_2O_3 (%)	K_2O (%)	MgO (%)	MnO (%)	Na_2O (%)	P_2O_5 (%)	SO_3 (%)	SiO_2 (%)	SrO (%)	TiO_2 (%)	LOI (%)	Nb (ppm)	Zr (ppm)
LLS1	18.78	0.075	0.48	0.01	6.235	2.09	1.53	0.035	1.11	0.105	0.05	66.04	0.02	0.765	2.295	0.765	240
LLS2																15	225
LLS3	17.30	0.09	0.8	0.01	5.42	2.25	1.47	0.03	1.64	0.1	0.04	67.81	0.03	0.76	2.06	15	266
LLS4																21	241
LLS6	20.11	0.08	0.38	0.01	6.52	2.03	2.02	0.03	0.88	0.1	0.02	64.99	0.01	0.77	1.95	18	243
LLS7																19	250
LLS8																19	242

Table DR4. Major X-ray fluorescence data for lake sediment samples. Samples with the LIT and NOB prefixes are from the LIT and NOB core sites, respectively (Fig. 1).

Sample ID	Age (kyr BP)	Al_2O_3 (%)	BaO (%)	CaO (%)	Cr_2O_3 (%)	Fe_2O_3 (%)	K_2O (%)	MgO (%)	MnO (%)	Na_2O (%)	P_2O_5 (%)	SO_3 (%)	SiO_2 (%)	SrO (%)	TiO_2 (%)	LOI (%)
LIT-IC-3.5-9.5	0.19	17.03	0.09	1.22	0.01	6.02	2.38	1.62	0.07	2.04	0.19	0.04	66.31	0.03	0.78	1.53
LIT-IC-34-40	0.29	16.45	0.1	1.36	0.02	5.91	2.47	1.54	0.04	2.19	0.25	0.02	67.64	0.03	0.74	1.41
LIT-IF-9-17	0.91	18.52	0.09	1.22	0.02	6.16	2.22	2.16	0.06	1.67	0.2	0.18	64.53	0.03	0.89	1.99
LIT-IF-47.5-55.5	1.04	15.89	0.1	1.46	0.01	4.29	2.55	1.38	0.04	2.43	0.11	0.05	69.44	0.04	0.68	0.89
LIT-IG-53-60	1.30	17.3	0.1	1.4	0.01	5.13	2.41	1.72	0.05	2.22	0.13	0.08	67.04	0.03	0.83	1.23
NOB-A2-24.5-27	16.4	15.36	0.09	1.26	<0.01	3.27	2.72	1.07	0.02	2.46	0.034	0	71.07	0.04	0.52	1.63
NOB-A2-54-57	16.4	15.67	0.09	1.57	<0.01	3.21	2.64	1.09	0.03	2.63	0.037	0	70.17	0.04	0.64	1.66
NOB-A4-16-20	20.5	15.1	0.09	1.61	0.01	2.76	2.74	1.01	0.02	2.73	0.049	0	71.69	0.04	0.5	1.03
NOB-A4-34-37	20.5	17.3	0.09	1.69	0.01	4.07	2.68	1.78	0.03	2.45	0.092	0	66.55	0.04	0.77	2.11
NOB-B40d-5-10	23.4	15.17	0.1	1.66	0.02	3.73	2.62	1.27	0.03	2.67	0.08	0.03	71.32	0.04	0.52	1.04
NOB-B50b-0-5	23.5	15.74	0.1	1.5	0.01	4.53	2.49	1.48	0.04	2.44	0.11	0.03	70.3	0.04	0.6	0.86
NOB-C80a-0-4.5	25.1	15.73	0.09	1.62	<0.01	5.31	2.69	1.48	0.05	2.6	0.094	0	68.38	0.04	0.74	1.18
NOB-B96c-5-9	25.7	15.16	0.1	1.8	0.01	3.83	2.62	1.26	0.04	2.74	0.08	0.03	70.8	0.04	0.51	0.7
NOB-B108d-0-2.5	27.0	14.98	0.09	2.11	<0.01	3.97	2.77	1.33	0.04	3.08	0.125	0	69.65	0.05	0.47	1.04
NOB-B124a-4.5-7.5	29.4	15.68	0.08	1.69	<0.01	5.56	2.68	1.54	0.07	2.49	0.134	0	67.11	0.04	0.59	1.61

Table DR5. Trace element X-ray fluorescence data for lake sediment samples. Samples with the LIT and NOB prefixes are from the LIT and NOB core sites, respectively (Fig. 1).

Sample ID	Age (kyr BP)	Nb (ppm)	Zr (ppm)
LIT-IA-5-7	0.02	15	242
LIT-IA-17-19	0.06	15	235
LIT-IC-3.5-9.5	0.19	17	243
LIT-IC-34-40	0.29	15	234
LIT-IE-33.5-35.5	0.75	19	254
LIT-IF-9-17	0.91	19	232
LIT-IF-47.5-55.5	1.04	15	232
LIT-IG-53-60	1.30	17	255
LIT-IJ-26-29	2.00	12	193
NOB-A2-24.5-27	16.4	11	165
NOB-A2-54-57	16.4	12	219
NOB-A4-16-20	20.5	10	158
NOB-A4-34-37	20.5	16	215
NOB-C12c-0-4	22.7	14	199
NOB-C20a-5-8	23.3	12	173
NOB-B40d-5-10	23.4	11	165
NOB-B50b-0-5	23.5	12	194
NOB-C71c-9-15	24.1	13	186
NOB-C80a-0-4.5	25.1	12	184
NOB-B90d-all	25.6	12	182
NOB-B96c-5-9	25.7	10	178
NOB-B104d-12-16	26.5	18	204
NOB-B108d-0-2.5	27.0	10	178
NOB-B124a-4.5-7.5	29.4	13	188

Table DR6. Grain size data for lake sediment samples. Clay, silt, fine sand, medium sand, and coarse to very coarse sand size classes are defined as 0.02 µm-3.89 µm, 3.90 µm-62.49 µm, 62.5 to 250 µm, 250-500 µm, and 500-2000 µm, respectively.

Sample ID	Age (kyr BP)	Clay (%)	Silt (%)	Fine Sand (%)	Medium Sand (%)	Coarse to Very Coarse Sand (%)
LIT-IA-5-7	0.02	7.09	48.86	33.11	8.84	2.06
LIT-IA-17-19	0.06	6.14	45.14	38.25	9.25	1.20
LIT-IC-3.5-9.5	0.19	5.61	45.73	34.02	11.57	3.04
LIT-IC-34-40	0.29	4.17	42.95	44.13	8.00	0.72
LIT-IE-33.5-35.5	0.75	5.85	72.64	20.10	0.83	0.55
LIT-IF-9-17	0.91	6.05	78.91	14.36	0.37	0.29
LIT-IF-47.5-55.5	1.04	1.74	30.12	53.69	12.43	2.01
LIT-IG-53-60	1.30	4.09	47.35	45.28	2.26	1.01
LIT-IJ-26-29	2.00	1.90	26.47	43.48	19.13	9.01
NOB-C12c-0-4	22.73	2.64	26.45	32.91	29.57	8.41
NOB-C20a-5-8	23.28	1.71	20.85	41.60	26.72	9.09
NOB-B40b-5-10	23.36	0.91	14.68	41.39	35.19	7.82
NOB-B50b-0-5	23.52	1.73	23.37	43.14	24.34	7.40
NOB-C71c-9-15	24.10	2.52	26.09	48.29	20.46	2.62
NOB-82d-6-10	25.40	5.07	44.69	43.70	5.50	1.01
NOB-B90d-ALL	25.60	0.93	16.97	26.07	37.66	18.36
NOB-94d-0-4	25.68	3.79	41.16	41.60	9.66	3.77
NOB-B96c-5-9	25.72	1.05	15.50	48.27	31.64	3.52
NOB-B96c-12-16	25.72	2.67	39.16	47.19	9.46	1.50
NOB-B104d-12-16	26.52	2.75	31.30	47.43	16.36	2.14
NOB-112a-8-11.5	27.42	6.49	56.32	31.87	2.93	2.36
NOB-B116d1-4	28.19	6.43	66.49	26.30	0.19	0.56
NOB-B136a-1-4	33.26	1.67	21.69	55.59	19.68	1.35
NOB-B136a-10-13	33.26	10.47	65.09	15.26	4.19	4.94
NOB-142b-6-9	35.30	37.84	54.54	5.46	0.34	1.78
NOB-B170a-7-11	42.77	12.20	74.02	11.66	0.40	1.67
NOB-B199d-4-7.5	46.99	6.04	43.11	34.97	10.93	4.92
NOB-B199d-7.5-11	46.99	20.78	74.51	1.26	0.44	2.92

Table DR7. X-ray fluorescence data for soil and lake sediment grain size separates.

Sample ID	Nb (ppm)	Zr (ppm)
NOB-B90d (LG sediment)		
0-63 µm	20	289
63-250 µm	11	158
250-500 µm	9	134
500-2000 µm	16	212
Mass-weighted Avg.		182
LLS8 (soil)		
0-63 µm	22	421
63-250 µm	16	241
250-500 µm	15	225
500-2000 µm	16	227
Mass-weighted Avg		264

Table DR8. Soil and bedrock bulk density measurements.

Sample ID	Density (g/cm^3)	Sample type
LLS2-T3-10bd	1.11	Soil
LLS2-T8-10bd	0.99	Soil
LLS6-20-25bd	1.04	Soil
LLS7-35-40bd	1.17	Soil
LLB13	2.28	Bedrock
LLB14	2.22	Bedrock
LLB15	2.23	Bedrock